SCIENTIFIC REPORTS

OPEN

SUBJECT AREAS:
PALAEOCLIMATE
PALAEOCEANOGRAPHY
GEOCHEMISTRY
GEOMORPHOLOGY

Received
7 March 2013

Accepted
3 June 2013

Published
20 June 2013

Correspondence and requests for materials should be addressed to D.D.-V. (david.dominguez@cenieh.es)

Early maximum extent of paleoglaciers from Mediterranean mountains during the last glaciation

D. Domínguez-Villar[1,2], R. M. Carrasco[3], J. Pedraza[4], H. Cheng[5,6], R. L. Edwards[6] & J. K. Willenbring[7]

[1]Centro Nacional de Investigación sobre la Evolución Humana (CENIEH), 09002 Burgos, Spain, [2]School of Earth and Environmental Sciences, University of Birmingham, Birmingham, UK, [3]Dpt. Ingeniería Geológica y Minera, Universidad de Castilla-La Mancha, 45071 Toledo, Spain, [4]Dpt. Geodinámica, Universidad Complutense de Madrid, 28040 Madrid, Spain, [5]Inst. of Global Environmental Changes, Xian Jiaotong University, 710049 Xian, China, [6]Dpt. Geology and Geophysics, University of Minnesota, 55455 Minneapolis (MN), USA, [7]Dpt. Earth and Environmental Sciences, University of Pennsylvania, 19104-6313 Philadelphia (PA), USA.

Mountain glaciers respond directly to changes in precipitation and temperature, thus their margin extent is a high-sensitivity climate proxy. Here, we present a robust ^{10}Be chronology for the glacier maximum areal extent of central Spain paleoglaciers dated at 26.1 ± 1.3 ka BP. These glaciers reached their maximum extent several thousand years earlier than those from central Europe due to the increased precipitation within a cold period between 25 to 29 ka BP, as confirmed by a local speleothem record. These paleoclimate conditions impacted the maximum extent of mountain glaciers along the western and central Mediterranean region. The cause and timing of the enhanced precipitation implies a southward shift of the North Atlantic Polar Front followed by storm tracks in response to changes in insolation via orbital parameters modulation. Thus, these mountain paleoglaciers from the Mediterranean region record an ocean-continent climate interaction triggered by external forcing.

The Mediterranean region has a westerly circulation due to its mid-latitude position, and therefore, its climate is directly impacted by the North Atlantic. During the last glaciation, the mid-latitudes of the North Atlantic witnessed the most significant changes in the surface ocean dynamics[1], which greatly affected the global climate. Therefore, the Mediterranean mountain paleoglaciers[2,3] record the ocean-continent climate interactions during the last glaciation in a critical location. However, there are only a limited number of locations with robust chronologies for the glacier maximum extent (GME) in the Mediterranean mountains to allow the identification of regional paleoclimate patterns (Fig. 1, Supplementary Table S1).

The paleoglaciers from the Spanish Central System have an ideal geologic and geomorphologic setting to provide a robust chronology for the regional GME (see supplementary information). Additionally, a U-Th dated paleoclimate record based on speleothems from the nearby Eagle Cave, provides information on the amount of precipitation supplied to the region during the period of interest, allowing our study to evaluate the impact of precipitation on the areal extent of the glaciers.

Many summits and plateaus of the Spanish Central System hosted glaciers during the last glacial period (Fig. 1), although they are absent today. The mountains are mostly composed of granite and gneiss rocks, which provided tills and erratics with boulders of great size[4] ideal for using the cosmogenic ^{10}Be exposure dating technique. The paleoglaciers from the region have a morphosedimentary record with differentiated homogeneous geomorphologic units[5]. The "Peripheral Deposits" (PD) is the unit that contains the GME, although also records later pulses or stages. The PD consists of a series of geomorphic indicators (i.e., moraines, boulders-belts and erratic strewn boulders). Frequently, this unit has a sequence of indicators (e.g., several parallel moraines) whereas the most external indicators represent the GME and the internal indicators record later fluctuations of the ice margin in which the glaciers were close to the GME extension (see supplementary information for further descriptions and illustrations of the PD). The overflow of ice on top of the plateaus or gentle slopes aside from fluvial or slope dynamics has favored the complete preservation of PD sequences in many lateral moraines. Therefore, recognition of these sites after detailed geomorphologic mapping minimizes the risk of misidentification of the GME.

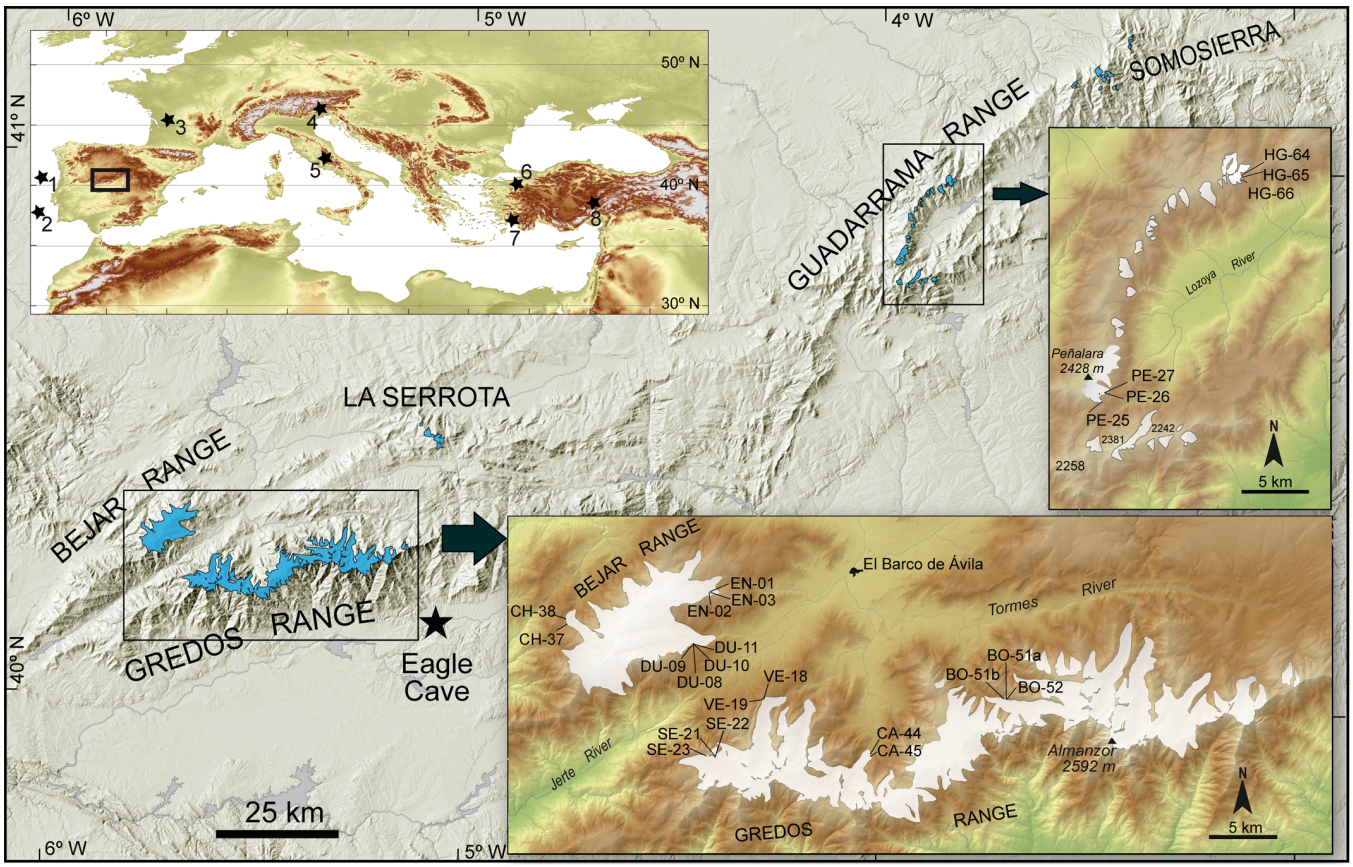

Figure 1 | Map of the Spanish Central System showing the limits of the paleoglaciers of the region during their maximum extension. Detailed sketches show the sampling sites for ^{10}Be. The inset map of the Mediterranean mountains shows the location of different sites discussed in the text: 1) MD95-2040[19], 2) MD95-2042[19], 3) Villars Cave[21], 4) Tagliamento amphitheater[12], 5) central Apennines[13], 6) Uludağ Mnt.[9], 7) Sandıras Mnt.[10], 8) Erciyes Mnt.[11]. Mapping of Béjar and Gredos glaciers after Pedraza *et al.*[5]. The digital elevation model used in this map is from the free access database of the IGN (www.ign.es).

Results

Nine paleoglaciers from the Béjar, Gredos and Guadarrama ranges were studied to determine the GME chronology and its replicability. Twenty-five samples were obtained from boulders deposited by the paleoglaciers in the PD unit (Supplementary Table S2). To minimize the bias of the age determination and to improve the accuracy of the ^{10}Be chronology, a specific erosion rate was applied to the age calculation for each sample. However, the effect of erosion on the calculated dates assuming no erosion differs less than 1.0% in relation to the reported dates using the modeled erosion rate (Supplementary Table S2). The samples were always collected from geomorphic indicators representing glacier edges. So, the dates reported are interpreted as ages of sedimentation that records the timing of the glacier pulse that reached that particular location. The dating results show two age clusters for the PD unit, which are confirmed to be statistically different subpopulations according to Kolmogorov-Smirnov test ($p = 0.00041$). Therefore, due to the clear statistical separation between the two age subpopulations and the occurrence of major climate events between both periods, we recognize two different glacier stages (Fig. 2; Fig. 3). The age of each stage results from the highest probability after the sum of the probability distribution functions (PDFs) of every sample, and the reported uncertainty is the standard error of the mean of the two compiled PDFs. The stage representing the GME has a depositional age of 26.1 ± 1.3 ka BP, and is found in the most external geomorphic indicators. The second stage has an age of 21.3 ± 0.7 ka BP and contains boulders from both, internal and external geomorphic indicators (Fig. 2; Fig. S2–S4). The chronology of the PD unit confirms the existence of an early GME in central Spain ($n = 6$ in 4 paleoglaciers) in comparison with glacier chronologies from central Europe: the glaciers from the northern Alps[6], the southern sector of the Scandinavian Ice Sheet[7] or the Great Britain-Irish Ice Sheet[8]. However, the second glacier stage recorded in central Spain ($n = 16$ in 8 glaciers) is in agreement with the central Europe and eastern Mediterranean GME glacier chronologies[9–11] and with secondary glacier stages in the mountain glaciers from the southern Alps[12] and the Apennines[13,14]. The PD unit has a limited extent (averaging <250 m along sequence traverses), and most of the record was accumulated during the later stage, which implies that during both stages the extents of the glaciers were similar. Thus, some geomorphic indicators identified as external have ages that do not correspond with the central Spain GME, which implies that boulders from a further glacier extent have not been preserved/identified on these paleoglaciers or that the ice margin of the later stage overrode the previous deposits at that particular location, illustrating the limited extent differences in some cases between both stages.

Two stalagmites from Eagle Cave, located only 10 km south of the Gredos Range, were U-Th dated (Supplementary Table S3) and their isotope signal was studied. The δ^{18}O record of the samples depends on several factors and its variability cannot be interpreted as the result of a single control (see supplementary information). However, most of the δ^{18}O variability depends on the amount of precipitation with the changes in moisture source (mostly accounting for differences in the seasonal ice cover in the North Atlantic),

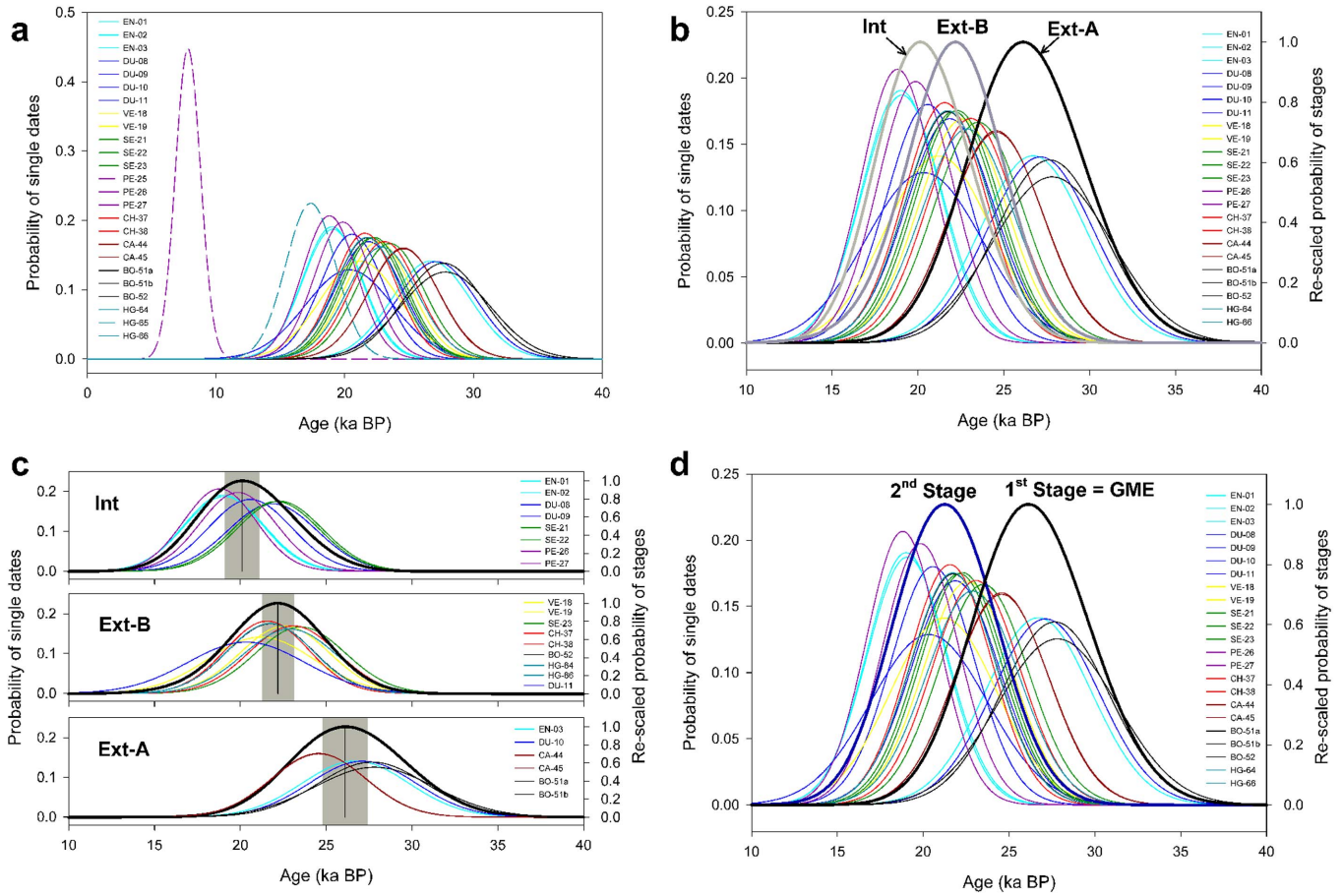

Figure 2 | Probability distribution functions (PDFs) of the ^{10}Be dates in PD unit of paleoglaciers from Béjar, Gredos and Guadarrama ranges. (a) PDFs of the ^{10}Be dates. Samples from each paleoglacier have different colours. Dashed lines represent discarded dates. (b) Cumulative PDFs for boulders (bold lines) from internal and external geomorphic indicators. Note that the dates of the external geomorphic indicators provide two subpopulations (Ext-A and Ext-B). PDFs of individual samples are also plotted. (c) Similar to (b) but divided in three panels in order to differentiate the individual samples in each subpopulation. The black vertical lines are the most probable age for each subpopulation and the grey bars are the standard error of the mean for each cumulative PDF. (d) PDFs of the two stages recorded in the PD unit (bold lines) together with the individual PDFs.

likely playing a secondary but significant role. Additionally, the mineralogy is a factor affecting the δ^{18}O signal during two particular periods around 24 and 30 ka BP when aragonite, instead of calcite, comprises most of the carbonate (Fig. S5). Thus, lower values in the δ^{18}O record are interpreted as wetter periods, with moisture source potentially contributing in part to the variability of this proxy (Fig. 3). During the Heinrich events H2 and H3, the climate in the region was extremely dry[15] as reflected by high δ^{18}O values and the presence of aragonite. The lower values of the δ^{18}O record between 25 to 29 ka BP when compared to the period 19 to 23 ka BP, in which the central Spain paleoglaciers record the second glacier stage, confirm that the climate was wetter in this region at the time of GME than during the second glacier stage. A similar paleoclimate pattern is recorded in other sites of the Iberian and the Italian peninsulas[16,17] supporting its regional influence over part of the Mediterranean.

Discussion

The extent of mid-latitude mountain glaciers depends on their long term mass balance. Therefore, glacier extent changes are related to persistent variations in their accumulation and/or ablation values. In general, the accumulation is primarily controlled by the cold season snow precipitation, while the ablation depends mostly on the warm season temperature, controlled in part by the energy received by the sun and modulated by the orbital parameters. At 40°N latitude, the integrated summer insolation (ISI) that affects the glacier ablation had a minimum at 27 ± 4 ka[18]. However, sea surface temperature (SST) offshore Iberia in the Atlantic Ocean was cooler during the period 19 to 23 ka BP than during the central Spain GME[19]. Even lower SSTs were recorded during Heinrich events, but particularly dry conditions associated with these periods[15] prevented the glaciers in southern Europe from reaching their GME[3]. In fact, the cause for an early GME in the Mediterranean region in comparison central Europe is thought to be related to a glacier mass balance dominated by increased precipitation rather than cooler temperatures[20]. Nevertheless, temperatures in southern Europe were so cold by 30 ka that in Villars Cave (southern France), the speleothems stop their growth due to continuous permafrost over the cave[21]. This local and regional paleoclimate context suggests that the optimal combination of wet and cold conditions that caused the paleoglaciers to reach their maximum extension were recorded in central Spain around 25–29 ka BP. Thus, the cooler and drier climate conditions recorded between 19 and 23 ka BP in comparison with the 25–29 ka BP period were responsible for glaciers of large dimensions in the region, but not enough for reaching the GME.

In order to investigate the causes of the wet period between Heinrich events H2 and H3 and to discard the existence of other periods suitable to record the GME, the regional paleoclimate context is shown in figure 4 up to the onset of the last glaciation at the end of marine isotope stage 5 (MIS5). During the 19–23 ka BP period, the North Atlantic Polar Front (PF) was at the latitude of Iberia[19]. The

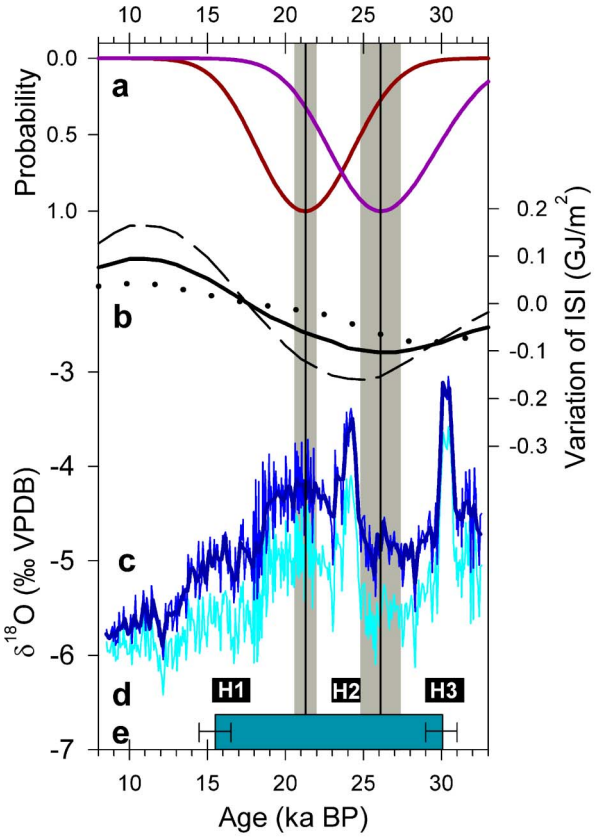

Figure 3 | Chronology of the PD in the Central Spain paleoglaciers and paleoclimate setting. (a) Probability distribution functions of the ^{10}Be ages for the two stages. Black vertical lines represent the stage ages with the grey vertical bars being the standard error of the mean. (b) ISI variability for 40°N[18] for most likely τ configurations; τ = 325 (dashed); 350 (solid) and 375 (dotted). (c) Eagle Cave δ^{18}O record (light blue) and ice volume corrected δ^{18}O record (dark blue) with a 0.2 ka filter (bold blue). The isotope ratio correction takes into account sea level changes by Peltier and Fairbanks[37] considering a rate of change of 0.06‰/10 m of sea level[38]. (d) Black rectangles labelled H1 to H3 refer to Heinrich events[39]. (e) Green rectangle corresponds with the period of lack of calcite deposition in Villars Cave (southern France) due to extreme cold conditions[21]. Error bars indicate U-Th ages uncertainty.

SST difference of the Ocean cores MD95-2040 and MD95-2042 located along the coast of Iberian margin in the North Atlantic reflects the proximity of the PF, where the thermal gradient is maximum[1]. During the past 80 ka, two periods of outstanding southern displacement of the PF are recorded: between 26–32 ka BP and 66–72 ka BP. The storm tracks over Europe followed these southern shifts since their energy is taken from the ocean thermal gradient[22,23]. The resulting climate setting provides more precipitation over most of the Mediterranean region, with the exception of the periods of extreme low SST during Heinrich events, which limited the moisture uptake[15]. Both periods of increased thermal gradient along the Iberian coast roughly match the minima in the ISI at 40°N, and are candidates to record the GME in the Mediterranean region. However, the continental temperatures in the early part of MIS4, when ISI conditions are minimal (72 ± 4 ka BP) were too mild compared with the later period (27 ± 4 ka BP), when conditions were then optimal to reach the GME in the region.

While the glacier records in central Europe reach their GME within the 19–23 ka period[6–8], paleoglaciers from central Iberia, southern Alps[12] and central Italy[13,14] record an early GME around 26 ka BP. In contrast, paleoglaciers from Turkey have shown a GME during the 19–23 ka BP period[9–11]. This difference is attributed to the intensification of the Siberian High during glacial times[24], which prevented the southward shifted storm track system to significantly impact continental Asia in the eastern Mediterranean, maintaining similar precipitation conditions between 20 and 30 ka BP in the region[25].

In the western and central Mediterranean, a persistent increase in the snow accumulation during the cold period from 25 to 29 ka BP caused mountain glaciers to reach their GME. This early GME in relation to glaciers from central Europe and the eastern Mediterranean is the result of differential precipitation distribution in the continent. The increased precipitation over part of the Mediterranean was the consequence of a southward shift of the storm tracks in response to ocean dynamics in the North Atlantic. The match of the limited seasonal amplitude determined by the lower obliquity and normalized orbital forcing[26,27] with the larger SST gradients along Iberian coast, suggests a substantial role of the winter sea ice cover in controlling the precipitation regime over the Mediterranean region. The paleoglaciers from central Europe and the eastern Mediterranean record their GME between 19 and 23 ka BP, a cold and relatively dry period in which mountain glaciers from the western and central Mediterranean also record important glacier stages, although these do not reach their GME. In any case, in all these regions the GME took place during the MIS2, fitting the period of minimum atmospheric CO_2, temperatures and relative sea level that commenced shortly after 30 ka BP[28].

Methods

Estimation of the erosion rate of boulder samples. We conducted a study of the regional erosion rates in mountains of central Spain in order to minimize the potential bias of the calculated ^{10}Be exposure ages in boulders deposited by glaciers and to improve accuracy of the chronology. To further constrain the erosion since deglaciation, we carried out calculations based on geomorphic evidence. Preservation of striations and polished surfaces due to glacial activity are uncommon in mountains from central Spain, but grooves and other signs of glacier abrasion are well represented. In these glacially abraded surfaces, the feldspar phenocrysts and quartz veins are resistant features due to differential weathering. Faint striations on top of these outstanding features are preserved under optimal conditions, supporting the assumption that their weathering since deglaciation is negligible. Therefore, the outstanding height of these features was considered to measure the erosion since deglaciation. Erosion was measured in ten sites along Béjar, Gredos and Guadarrama ranges. Selected sites are in top sections of *roches moutonnées* where concentrated erosion due to water runoff or fluvial activity is unlikely. Ponds or other sites of potential rainwater accumulation were avoided. Average erosion in each station was considered as the mean of fifty measures in different spots. To calculate the erosion rate a deglaciation age for each sampling site was considered. The deglaciation stage of the studied sites was established after regional mapping[5] and available regional chronologies[29–32]. Two different deglaciation stages with arbitrary deglaciation ages of 15 ± 1 and 19 ± 1 ka cover the location of all the studied sites. Although age determination for each stage introduces a significant uncertainty, the constraint of deglaciation on these mountains to short periods makes erosion rates less vulnerable to age uncertainties. One of the sites shows high erosion rate (3.58 ± 1.27 mm·ka^{-1}) in agreement with field observations. The abundant presence of xenoliths in these rock suggest that its particular petrologic properties make it prone to heavy weathering in comparison with the rest of granites and gneisses analyzed. This observation is corroborated by tests done with a Schmidt hammer that provided Q-values of 37.4 ± 2.8 (dimensionless) on the heavily weathered boulders in comparison with the rest of analyzed samples with Q-values from 47.6 ± 2.1 to 53.2 ± 2.1. These heavily weathered boulders are easily recognizable in the field and they were discarded for ^{10}Be exposure dating sampling. For the rest of the sites studied, the erosion rate was between 0.58 ± 0.16 and 0.29 ± 0.08 mm·ka^{-1}. These low erosion rates for the studied mountain ranges are in good agreement with previous weathering studies in weathering pits[33] and the preservation of abrasion features since deglaciation. There is a positive correlation of erosion rate and elevation ($r^2 = 0.94$; $p < 0.01$) following a linear relationship (Fig. S6). Therefore, this relationship was used to model the erosion rate for every sampled boulder and correct the ^{10}Be exposure ages. Although this method for estimating erosion rates has inherent limitations, it improves the accuracy of the ^{10}Be exposure ages in comparison with traditional assumptions for erosion rate. Thus, we avoid assuming an unrealistic zero erosion since deglaciation, or generalizing regional erosion rates.

Calculation of ^{10}Be dates and chronology of PD stages. The samples collected from PD unit followed standard procedures of sample preparation for ^{10}Be dating[34]. The ^{10}Be/^{9}Be ratio was measured at PRIME laboratory. Sample shielding factors and sample thickness were measured in the field and incorporated in the calculations. We suspect that boulders remained windswept due to their height, and so snow cover

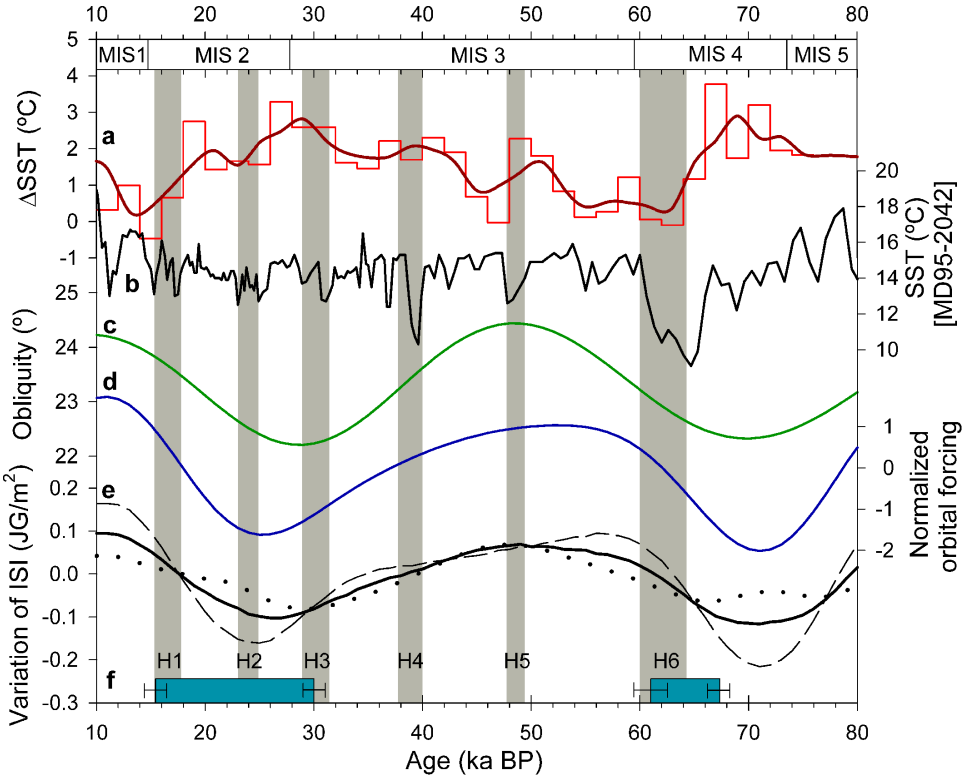

Figure 4 | Paleoclimate context affecting paleoglaciers in the Mediterranean region. (a) SST difference between cores MD95-2042 and MD95-2040[19] at 2 ka intervals (thin red) with a 6 ka filter (bold red). (b) SST at MD95-2042[19]. (c) Obliquity[26]. (d) Normalized orbital forcing[27]. (e, f) ISI variability and period of calcite deposition in Villars Cave as in figure 3. Heinrich events H1 to H6 are represented as vertical grey bars[39].

estimates were not considered. The coordinates of samples were taken with a GPS in the field, and their location was improved by relocating the boulders in a 5 m cell resolution digital elevation model with 0.25 m pixel size resolution orthophoto incorporated, in which individual boulders were identified. Calculation of the production rate and ages was done with the CRONUS-Earth online calculator v2.2[35]. Because there are no production rates for the specific area of our research, we have used the standard scaling and accepted ^{10}Be production rates in Balco *et al.*[35] and chosen to report the external uncertainty given the small discrepancies between the scaling methods available. Our results and conclusions regarding the early GME and two phases of glacial activity are insensitive to which of the scaling scheme we choose. Here, we report our data based on Lifton *et al.*[36] scaling scheme given in the CRONUS-Earth online calculator that includes temporal variations in the cosmic ray flux. Ages are provided in ka BP (before present), where present is considered the year 1950 (i.e., ages provided by the online calculator were shifted 58 to 61 years depending on the sampling year) in order to match other chronologies. Two sets of ages are displayed in Table S2: considering no erosion rate and the modelled erosion rate. The chronology of this paper consider the modelled ages, although differences are $<1\%$ in relation to those that consider zero erosion rates.

The modelled age results and the external uncertainties (1σ) were used to calculate the probability distribution functions (PDFs) of each date. From the 25 dates calculated 2 of them (PE-25 and HG-65) were considered unreliable due to lack of overlapping (within 1σ external uncertainty) with samples from the same geomorphic indicator. Most likely, these samples suffered some unexpected rotation or surficial erosion after exposition that made their ages younger than other boulders in the same paleoglacier sequence. These dates are discarded in further calculations.

The distribution of dates of PD unit shows two clear subpopulations in the PDFs (Fig. 2A). The dates are categorized based on the geomorphologic context of the sampled boulders (internal or external geomorphic indicators) along the sequences of the PD unit, and the cumulative PDFs have been calculated using k-means clustering to split the data (Fig. 2B and Fig. 2C). The internal geomorphic indicators provided dates within one subpopulation with most probable age at 20.1 ka BP ("Int" in Fig. 2). The external geomorphic indicators provided dates distributed in two subpopulations, with most probable ages at 26.1 and 22.2 ka BP ("Ext-A" and "Ext-B" respectively in Fig. 2). The Kolmogorov-Smirnov test was applied to evaluate if these populations are statistically different. Thus, the two subpopulations found on the external geomorphic indicators (Ext-A and Ext-B) belong to two different populations ($p = 0.00036$), whereas the younger subpopulation of dates from the external geomorphic indicators (Ext-B) and the dates from the internal geomorphic indicators (Int) can be considered to belong to the same population ($p = 0.1441$). Therefore, the dates from the younger subpopulation of external geomorphic indicators (Ext-B) and the dates from internal geomorphic indicators (Int) were merged in a single population with most probable age of 21.3 ka BP (Fig. 2D), which is statistically different from the subpopulation of most probable age of 26.1 ka BP ($p = 0.00041$).

1. Pflaumann, U. *et al.* Glacial North Atlantic: sea-surface conditions reconstructed by GLAMAP 2000. *Paleoceanography* **18**, 1065 (2003).
2. Hughes, P. D., Woodward, J. C. & Gibbard, P. L. Quaternary glacial history of the Mediterranean mountains. *Prog. Phys. Geogr.* **30**, 334–364 (2006).
3. Hughes, P. D. & Woodward, J. C. Timing of glaciation in the Mediterranean mountains during the last cold stage. *J. Quat. Sci.* **23**, 575–588 (2008).
4. Pedraza, J. in *Geomorfología de España* (ed. Gutierrez Elorza, M.) 63–100 (Rueda, 1994).
5. Pedraza, J., Carrasco, R. M., Domínguez-Villar, D. & Villa, J. Late Pleistocene glacial evolutionary stages in the Gredos mountains (Iberian Central System). *Quat. Int.* in press.
6. Ivy-Ochs, S. *et al.* Chronology of the last glacial cycle in the European Alps. *J. Quat. Sci.* **23**, 559–573 (2008).
7. Rinterknecht, V. R. *et al.* The last deglaciation of the southeastern sector of the Scandinavian Ice Sheet. *Science* **311**, 1449–1452 (2006).
8. Ballantyne, C. K. Extent and deglacial chronology of the last British-Irish ice Sheet: implication of the exposure dating using cosmogenic isotopes. *J. Quat. Sci.* **24**, 515–534 (2010).
9. Zhano, C., Akçar, N., Kubik, P. W. & Schlüchter, C. Chronology of Late Pleistocene glacier variations at the Uludağ Mountain, NW Turkey. *Quat. Sci. Rev.* **29**, 1173–1187 (2010).
10. Sarıkaya, M. A., Zreda, M., Çiner, A. & Zweck, C. Cold and wet Last Glacial Maximum on Mountain Sandıras, SW Turkey, inferred from cosmogenic dating and glacier modeling. *Quat. Sci. Rev.* **27**, 769–780 (2008).
11. Sarıkaya, M. A., Zreda, M. & Çiner, A. Glaciations and paleoclimatic variations on Mount Erciyes, central Turkey, since Last Glacial Maximum, inferred from ^{36}Cl cosmgenic dating and glacier modeling. *Quat. Sci. Rev.* **28**, 2326–2341 (2009).
12. Monegato, G. *et al.* Evidence of a two-fold glacial advance during the last glacial maximum in the Tagliamento end moraine system (eastern Alps). *Quat. Res.* **68**, 284–302 (2007).
13. Giraudi, C. & Frezzotti, M. Late Pleistocene glacial events in the central Apennines, Italy. *Quat. Res.* **48**, 280–290 (1997).
14. Giraudi, C. The Campo Felice late Pleistocene glaciation (Apennines, central Italy). *J. Quat. Sci.* **27**, 432–440 (2012).
15. Sánchez-Goñi, M. F. *et al.* Contrasting impacts of Dangaard-Oeschger events over a western European latitudinal transect modulated by orbital parameters. *Quat. Sci. Rev.* **27**, 1136–1151 (2008).

16. Valero-Garcés, B. L. *et al.* Paleohydrology flucuations and stepper vegetation during the last glacial maximum in the central Ebro valley (NE Spain). *Quat. Int.* **122**, 43–55 (2004).
17. Allen, J. R. M. *et al.* Rapid environmental changes in southern Europe during the last glacial period. *Nature* **400**, 740–743 (1999).
18. Huybers, P. Early Pleistocene glacial cycles and integrated summer insolation forcing. *Science* **313**, 508–511 (2006).
19. Pallier, D. & Bard, E. High frequency palaeoceanographic changes during the past 140000 yr recorded by he organic matter in sediments of the Iberian margin. *Palaeogeogr. Palaeoclimatol. Palaeoecol.* **181**, 431–452 (2002).
20. Florineth, D. & Schlüchter, C. Alpine evidence for atmospheric circulation patterns in Europe during the Last Glacial Maximum. *Quat. Res.* **54**, 295–308 (2000).
21. Genty, D. *et al.* Isotopic characterization of rapid climatic events during OIS3 and OIS4 in Villars Cave stalagmites (SW France) and correlation with Atlantic and Mediterranean pollen records. *Quat. Sci. Rev.* **29**, 2799–2820 (2010).
22. Kutzbach, J. E. & Guetter, P. J. The influence of changing orbital parameters and surface boundary conditions on climate simulations for the past 18000 years. *J. Atmos. Sci.* **43**, 1726–1759 (1986).
23. Woollings, T., Gregory, J. M., Pinto, J. G., Reyers, M. & Brayshaw, D. J. Response of the North Atlantic storm track to climate change shaped by ocean-atmosphere coupling. *Nature-Geosci.* **5**, 313–317 (2012).
24. Mayewski, P. A. *et al.* Major features and forcing of high-latitude northern atmospheric circulation using a 110,000-year-long glaciochemical series. *J. Geophys. Res.* **102**, 26345–26366 (1997).
25. Bar-Matthews, M. *et al.* Sea-land oxygen relationships from planktonic foraminifera and speleothems in the Eastern Mediterranean region and their implication for paleorainfall during interglacial intervals. *Geochim. Cosmochim. Acta* **67**, 3181–3199 (2003).
26. Berger, A. L. Long-term variations of Daily insolation and Quaternary climatic changes. *J. Atmos. Sci.* **35**, 2362–2367 (1978).
27. Huybers, P. Combined obliquity and precession pacing of late Pleistocene deglaciations. *Nature* **480**, 229–232 (2011).
28. Clark, P. U. *et al.* The last Glacial Maximum. *Science* **325**, 710–714 (2009).
29. Palacios, D., de Marcos, J. & Vázquez-Selem, L. Last Glacial Maximum and deglaciation of Sierra de Gredos, central Iberian Peninsula. *Quat. Int.* **233**, 16–26 (2011).
30. Palacios, D., de Andrés, N., de Marcos, J. & Vázquez-Selem, L. Glacial landforms and their paleoclimatic significance in Sierra de Guadarrama, Central Iberian Península. *Geomorphology* **139–140**, 67–78 (2012).
31. Palacios, D., Andrés, N., de Marcos, J. & Vázquez-Selem, L. Maximum glacial advance and deglaciation of the Pinar Valley (Sierra de Gredos, central Spain) and its significance in the Mediterranean context. *Geomorphology,* in press.
32. Carrasco, R. M., Pedraza, J., Domínguez-Villar, D., Villa, J. & Willenbring, J. K. The plateau glacier in the Sierra de Béjar (Iberian Central System) during its maximum extent. Reconstruction and chronology. *Geomorphology,* in press.
33. Domínguez-Villar, D., Razola, L., Carrasco, R. M., Jennings, C. E. & Pedraza, J. Weathering phases recorded by gnammas Developer since last glaciation at Serra da Estrela, Portugal. *Quat. Res.* **72**, 218–228 (2009).
34. Gosse, J. C. & Phillips, F. M. Terrestrial in situ cosmogenic nuclides: theory and application. *Quat. Sci. Rev.* **20**, 1475–1560 (2001).
35. Balco, G., Stone, J. O., Lifton, N. A. & Dunai, T. J. A complete and easily accessible means of calculating surface exposure ages or erosion rates from ^{10}Be and ^{26}Al measurements. *Quaternary Geochronology* **3**, 174–195 (2008).
36. Lifton, N. A. *et al.* Addressing solar modulation and long-term uncertainties in scaling secondary cosmic rays for in situ cosmogenic nuclide applications. *Earth Planet. Sci. Lett.* **239**, 140–161 (2005).
37. Peltier, W. R. & Fairbanks, R. G. Global glacial ice volume and Last Glacial Maximum duration from an extended Barbados sea level record. *Quat. Sci. Rev.* **25**, 3322–3337 (2006).
38. Schrag, D. P. *et al.* The oxygen isotopic composition of seawater during the Last Glacial Maximum. *Quat. Sci. Rev.* **21**, 331–342 (2002).
39. de Abreu, L. *et al.* Millennial-scale oceanic climate variability off the western Iberian margin during the last two glacial periods. *Mar. Geol.* **196**, 1–20 (2003).

Acknowledgements

This research received funds from the Ministerio de Ciencia e Innovación of the Spanish Ministry (CGL2008-03396/BTE) and the Junta de Comunidades de Castilla-La Mancha (PII1I09-0138-6113). We would like to thank Wang, Y. and Kong, X. (Nanjing Normal University), and Fairchild, I.J. (University of Birmingham) for carbonate and rainwater stable isotope analytical support respectively.

Author contributions

R.M.C. and J.P. provided geomorphologic mapping. Sampling for ^{10}Be dating was done by R.M.C., J.P., D.D.V. and J.K.W and the later conducted the analyses. D.D.V., H.C. and R.L.E. were responsible for speleothem U-series analyses. D.D.V. wrote the paper with contributions from J.K.W.

Additional information

Supplementary information accompanies this paper at http://www.nature.com/scientificreports

Competing financial interests: The authors declare no competing financial interests.

How to cite this article: Domínguez-Villar, D. *et al.* Early maximum extent of paleoglaciers from Mediterranean mountains during the last glaciation. *Sci. Rep.* **3**, 2034; DOI:10.1038/srep02034 (2013).